Imaging Prostate Cancer with ^{11}C-Choline PET/CT

Sven N. Reske[1], Norbert M. Blumstein[1], Bernd Neumaier[1], Hans-Werner Gottfried[2], Frank Finsterbusch[1], Darius Kocot[1], Peter Möller[3], Gerhard Glatting[1], and Sven Perner[3]

[1]Department of Nuclear Medicine, University of Ulm, Ulm, Germany; [2]Department of Urology, University of Ulm, Ulm, Germany; and [3]Department of Pathology, University of Ulm, Ulm, Germany

The ability of ^{11}C-choline and multimodality fusion imaging with integrated PET and contrast-enhanced CT (PET/CT) was investigated to delineate prostate carcinoma (PCa) within the prostate and to differentiate cancer tissue from normal prostate, benign prostate hyperplasia, and focal chronic prostatitis. **Methods:** All patients with PCa gave written informed consent. Twenty-six patients with clinical stage T1, T2, or T3 and biopsy-proven PCa underwent ^{11}C-choline PET/CT after intravenous injection of 1,112 ± 131 MBq ^{11}C-choline, radical retropubic prostatovesiculectomy, and standardized prostate tissue sampling. Maximal standardized uptake values (SUVs) of ^{11}C-choline within 36 segments of the prostate were determined. PET/CT results were correlated with histopathologic results, prostate-specific antigen (PSA), Gleason score, and pT stage. **Results:** The SUV of ^{11}C-choline in PCa tissue was 3.5 ± 1.3 (mean ± SD) and significantly higher than that in prostate tissue with benign histopathologic lesions (2.0 ± 0.6; $P < 0.001$ benign histopathology vs. cancer). Visual and quantitative analyses of segmental ^{11}C-choline uptake of each patient unambiguously located PCa in 26 of 26 patients and 25 of 26 patients, respectively. A threshold SUV of 2.65 yielded an area under the receiver-operating-characteristic (ROC) curve of 0.89 ± 0.01 for correctly locating PCa. The maximal ^{11}C-choline SUV did not correlate significantly with PSA or Gleason score but did correlate with T stage ($P = 0.01$; Spearman $r = 0.49$). **Conclusion:** ^{11}C-Choline PET/CT can accurately detect and locate major areas with PCa and differentiate segments with PCa from those with benign hyperplasia, chronic prostatitis, or normal prostate tissue. The maximal tumoral ^{11}C-choline uptake is related to pT stage.

Key Words: prostate carcinoma; ^{11}C-choline; PET/CT

J Nucl Med 2006; 47:1249–1254

Prostate carcinoma (PCa) is the most common life-threatening cancer in men. In 2005, 232,090 new cases were estimated, and approximately 30,350 men were expected to die from PCa in the United States (*1*). Small carcinomas are present in about 30% of men between 30 and 40 y old and in 64% between 60 and 70 y old (*1*). The accuracy of clinical examination, ultrasonography, and current radiographic techniques for detecting localized, curable PCa is limited, and an accurate imaging method of PCa within the prostate gland is needed.

Molecular imaging approaches using ^{11}C- or ^{18}F-labeled choline derivatives and PET have been used for detecting primary or relapsing PCa (*2–4*), based on increased content of phosphorylcholine (*5,6*), upregulated key enzymes of choline metabolism (*7–9*), increased phosphatidylcholine turnover, and metabolic flux of radiolabeled choline through phospholipid biosynthesis and degradation in PCa (*7–10*). ^{11}C-Choline has proven to be an appropriate probe for noninvasive imaging of PCa deposits in patients (*11–13*).

Several authors have shown that ^{11}C-choline is rapidly and preferentially taken up in PCa and its nodal and distant metastases (*2,10,14–18*). ^{11}C- and ^{18}F-labeled choline derivatives have a high sensitivity for locating primary PCa to the correct prostate lobe or sextant (*17,19*). Other investigators have reported high ^{18}F-fluoromethylcholine uptake both in benign prostate hyperplasia (BPH) and in PCa (*20*). In most studies, however, imaging results were verified only by comparing results of prostate biopsy (*19,21*) or histopathology (*22*) in the correct lobe (*17*) or sextant (*19,21,22*) of the prostate gland.

Therefore, we examined the capability of ^{11}C-choline and multimodality fusion imaging with integrated PET and contrast-enhanced CT (PET/CT) to delineate PCa within the prostate and to differentiate cancerous tissue from normal prostate, benign prostate hyperplasia, and focal chronic prostatitis. The purpose of our study was to assess the detection rate for regional involvement of the prostate with PCa through PET/CT using ^{11}C-choline as the imaging probe.

MATERIALS AND METHODS

The local ethics committee of our university and the national radiation protection authorities approved our study. All patients with PCa gave written informed consent.

Patients

An unselected population of 26 patients with resectable PCa as assessed by prostate-specific antigen (PSA), digital rectal examination, endorectal sonography, and standardized ultrasound-guided

Received Feb. 15, 2006; revision accepted Apr. 21, 2006.
For correspondence or reprints contact: Sven N. Reske, MD, Department of Nuclear Medicine, University of Ulm, Robert-Koch-Straße 8, D-89081 Ulm, Germany.
E-mail: sven.reske@uniklinik-ulm.de

sextant core biopsy was enrolled in this study between February 2002 and June 2004. In this period, 111 patients were scheduled for potential resective surgery of the prostate at the local urological department. Of these, 24 patients were excluded because of inadequate tissue sampling of the prostate, 30 patients refused resective surgery, and 31 patients were scheduled for nonsurgical therapies after complete clinical staging. Inclusion criteria were biopsy-proven PCa, clinical stage T1, T2, or T3 before surgical intervention, and standardized prostate tissue sampling after radical retropubic prostatevesiculectomy. ^{11}C-Choline PET/CT was done between 12 and 343 d after biopsy and between 1 and 50 d before radical retropubic prostatevesiculectomy. No patient was on antiandrogen medication or had clinical signs of acute prostatitis. PSA plasma concentration on the day of the ^{11}C-choline PET/CT study was determined (Hybritec assay; Table 1).

^{11}C-Choline PET/CT

^{11}C-Choline was synthesized according to the loop methylation method of Wilson et al. (*23*). ^{11}C-Choline PET/CT was performed after 5–8 h of fasting with an integrated PET/CT scanner (Discovery LS; GE Healthcare) following intravenous injection of 1,112 ± 131 MBq ^{11}C-choline. PET images were acquired 5–10 min after injection starting from the distal margin of the pelvic floor with a 3-min acquisition time per bed position (*20*). Contrast-enhanced CT (140 kV, 160 mAs, pitch 1.5) was acquired with 120 mL nonionic contrast agent given intravenously as a bolus (Ultravist; Schering) immediately before the PET acquisition. PET images were reconstructed with the iterative reconstruction ordered-subset expectation maximization likelihood algorithm of the manufacturer after attenuation correction based on the CT dataset. Consecutive transverse PET/CT slices of 4.25-mm thickness were generated.

Surgery and Histopathology

All patients underwent standardized radical retropubic prostatevesiculectomy in conjunction with pelvic lymphadenectomy according to current guidelines (*24*). Here, we focus on the detection of PCa within the prostate in relation to histopathologic examination.

The resected prostate was weighed and the surface was marked with ink followed by standard formalin fixation for 24 h. The urethral (apical) and the vesical (basal) margins (about 3–4 mm in thickness) were taken and sectioned parasagitally at 3- to 4-mm intervals, perpendicular to the marked surface. Then, the prostate was serially sectioned at 3- to 4-mm intervals perpendicular to the long axis from apical to basal regions of the gland until the junction of the seminal vesicles was reached. The transition zone from prostate gland to seminal vesicles was embedded in separate cassettes, one for each side. The slices were further formalin fixed and submitted for paraffin embedding. Then, microslices were placed on glass slides and stained with hematoxylin and eosin.

Representative slices from the middle of the basal, intermediate, and apical part of the prostate were selected for comparison with corresponding PET/CT slices (Fig. 1). Care was taken to correctly align PET/CT and histopathologic slices. Experienced pathologists (>10 y experience) performed histopathologic examinations. Tumor staging was performed according to the guidelines of the International Union Against Cancer (*25*).

PET/CT and histologic slides of the prostate were analyzed in 6 peripheral and 6 central segments, resulting in 36 segments evaluated in each patient (Fig. 1). In total, 936 histologic segments were analyzed for presence of normal prostate tissue, BPH, focal prostatitis (FP), or PCa.

TABLE 1
Characteristics of 26 Patients in Study

Characteristic	Value
Age (y)	
Mean	64
Range	53–74
Serum PSA (μg/L)	
Mean	14.4
Range	2.8–64.3
Gleason score*	
Mean	6.7
Range	4–9
T stage	
pT2a	9
pT2b	2
pT2c	5
pT3a	5
pT3b	3
pT4	2

*Gleason score can range from 2 to 10, with higher scores indicating more aggressive disease.

Image Analysis

The PET/CT scans were visually assessed by 2 experienced nuclear physicians, who were unaware of clinical data and results of previous imaging studies. The criterion for diagnosing PCa on visual analysis was mono- or multifocal ^{11}C-choline uptake in the prostate gland defined by CT as significantly higher than ^{11}C-choline uptake in periprostatic soft tissue, in pararectal fat tissue, or in pelvic muscles (*19,22*). Care was taken to differentiate prostatic ^{11}C-choline uptake from rectal activity. Because of limited spatial resolution of the PET/CT system (5-mm full width half maximum)—limited delineation of prostate and lower margins of the seminal vesicals and potential movements of prostate (*26*) between CT and PET acquisition—we did not try to determine capsular invasion on the PET/CT images.

For quantitative assessment, the middle slice from the apical, intermediate, and basal part of the prostate was selected and used for comparative analysis of PET/CT with the corresponding histopathologic slide (Fig. 1). Each PET/CT slice was divided into 12 segments as shown in Figure 1. The ^{11}C-choline maximal standardized uptake value (SUV_{max}) in each segment was determined using a circular, 1-cm (diameter) region of interest. SUV is defined as the measured activity concentration divided by the injected radioactivity normalized to body weight (*19*) and was determined by one of us.

^{11}C-Choline uptake was compared in segments with normal prostate tissue, BPH, prostatitis, mixed benign findings (normal tissue, BPH, prostatitis) and in segments with PCa. In addition, a subgroup analysis was performed in those segments that contain tumor foci greater than 5 mm in diameter.

Statistical Analysis

Data are presented as mean ± SD. SUVs between groups were compared using the Mann–Whitney *U* test. Differences were considered to indicate statistical significance for 2-tailed *P*

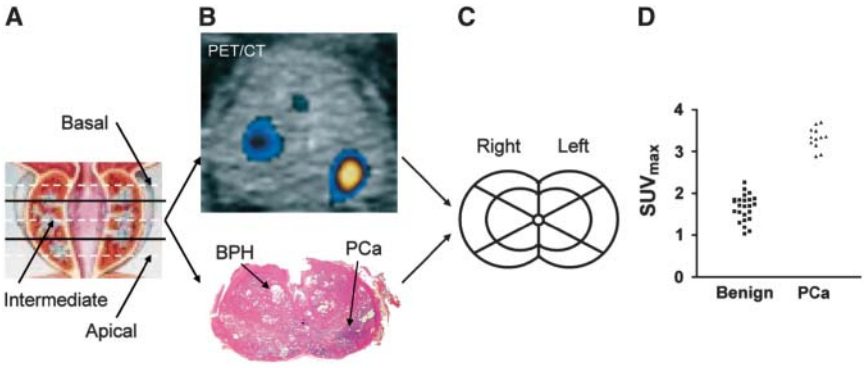

FIGURE 1. (A–D) Image analysis of ^{11}C-choline PET/CT and histopathology. (A) Assessed cutting planes of prostate are indicated as dashed lines. (B) ^{11}C-Choline PET/CT slice from middle third of prostate: corresponding transversal whole-gland section (hematoxylin and eosin). (C) Segmental allocation. (D) Scatter plot of ^{11}C-choline maximal standardized uptake value (SUV_{max}) of all 36 segments of this patient. Tumor stage was pT2a; ^{11}C-choline PET/CT localized PCa correctly to left lower peripheral segment (arrow in B). Scatter plot in D shows higher ^{11}C-choline SUV_{max} in segments with PCa than in those with benign histopathologic lesions.

values < 0.05. Statistical analysis was performed with GraphPad Prism software, version 3.00 (GraphPad Software).

Accuracy was defined as the percentage of all segments in which the SUV_{max} correctly predicted the presence or absence of PCa, calculated with the following equation: (true-positive + true-negative) ÷ (number of segments).

The receiver-operating-characteristic (ROC) analysis was performed by calculating the sensitivity and specificity for a sample of threshold values of the SUV_{max}. The readers had no knowledge of the histopathologic diagnosis during determination of the SUV_{max} for the segments. A binormal ROC curve was fitted to the SUV_{max} values with a maximum likelihood estimation (*27*). The diagnostic accuracy of correctly identifying the segmental location of PCa was evaluated by calculating the area A under the ROC curve using the ROCKIT software (Charles E. Metz, University of Chicago, Chicago, IL).

RESULTS

Characteristics of Patients

Twenty-six patients with pathologically proven PCa were enrolled in the study (Table 1). Patients had a biopsy-proven diagnosis of PCa on 54 ± 61 d (median, 44 d; range, 12–343 d) before the PET/CT study and underwent radical retropubic prostatovesiculectomy within a mean time of 11 ± 13 d (median, 4.5 d; range, 1–50 d) between PET/CT and surgery. The mean prostate weight was 43 ± 18 g (range, 25–102 g). All patients had adenocarcinoma. The Gleason score was 6.7 (mean, range 4–9).

Diagnosis

Two experienced observers—unaware of clinical data and results of previous imaging studies, but with full knowledge of a prostate biopsy result positive for PCa—visually assessed PET/CT images and judged 26 of 26 patients positive for PCa. Typical findings of focal or multifocal ^{11}C-choline uptake in representative PET/CT slices are shown in Figure 2, respectively. In 1 of 26 patients, infiltration into the bladder wall was suspected from the ^{11}C-choline PET/CT study. This patient had a pT4 tumor stage on histopathologic examination. Microscopic bladder infiltration in the other patient with a pT4 tumor stage was not detected with ^{11}C-choline PET/CT.

Histopathology showed 66, 147, 33, 241, and 449 segments with normal prostate tissue, BPH, prostatitis, BPH mixed with focal prostatitis, or PCa, respectively. In 177 segments, tumor foci of >5 mm in diameter were observed by histophathology. ^{11}C-Choline uptake in PCa (SUV_{max}, 3.5 ± 1.3; mean ± SD) was significantly higher ($P <$ 0.001) than that in normal prostate tissue (1.7 ± 0.5), BPH

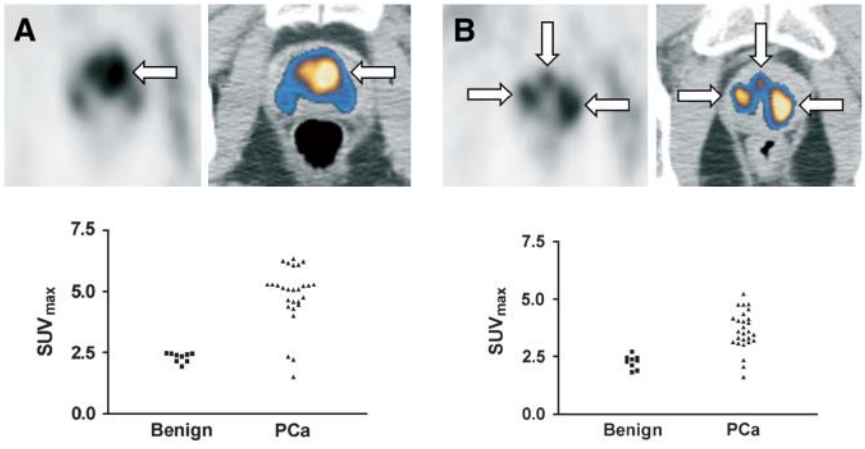

FIGURE 2. Focal (A) and multifocal (B) distribution of PCa within prostate gland (arrows). Scatter plots of segmental ^{11}C-choline SUV_{max} show higher ^{11}C-choline SUV_{max} in most segments with PCa compared with segments with benign histopathologic lesions.

(2.0 ± 0.6), focal prostatitis (2.1 ± 0.6), BPH mixed with focal prostatitis (2.1 ± 0.7), and all segments with benign histopathologic lesions together (2.0 ± 0.6). In the 177 segments with tumor foci of >5-mm diameter, SUV_{max} was 3.8 ± 1.5. ^{11}C-Choline SUVs in BPH, focal prostatitis, and BPH mixed with focal prostatitis were not significantly different (Fig. 3; however, they were each significantly larger than the SUV_{max} of normal tissue ($P < 0.001$).

Scatter plots of segmental ^{11}C-choline SUV in 17 of 26 patients showed a higher ^{11}C-choline uptake in >50% of segments with PCa compared with the maximal SUV_{max} of the segments with benign histopathologic lesions (Fig. 4). In 6 of 26 patients, ^{11}C-choline uptake was higher in 28%–42% of segments with PCa; in 1 of 26 patients, ^{11}C-choline uptake was highest in a segment with BPH (Fig. 4).

The reliability of segmental ^{11}C-choline uptake for detecting PCa was analyzed using ROC analysis. The area under the ROC curve for diagnosing PCa using segmental ^{11}C-choline SUV_{max} was 0.89 ± 0.01 (Fig. 5). For a threshold SUV_{max} of 2.65 chosen to yield the maximal accuracy, we obtained a sensitivity of 0.81 (363/449), a specificity of 0.87 (426/487), a positive predictive value of 0.86 (363/424), a negative predictive value of 0.83 (426/512), and an accuracy of 0.84 (789/936). The area under the ROC curve for 177 segments with tumor foci of >5 mm and a threshold value of SUV_{max} of 3.05 was 0.93. The sensitivity, specificity, positive predictive value, and negative predictive value for this subgroup of segments with PCa were 0.75, 0.95, 0.84, and 0.91, respectively. The SUV_{max} of small tumors (i.e., pT2a; $n = 9$ patients) was significantly less than that of larger tumors (i.e., pT2a; $n = 17$ patients): SUV_{max} = 3.8 ± 0.3 vs. 5.3 ± 1.7 ($P = 0.004$).

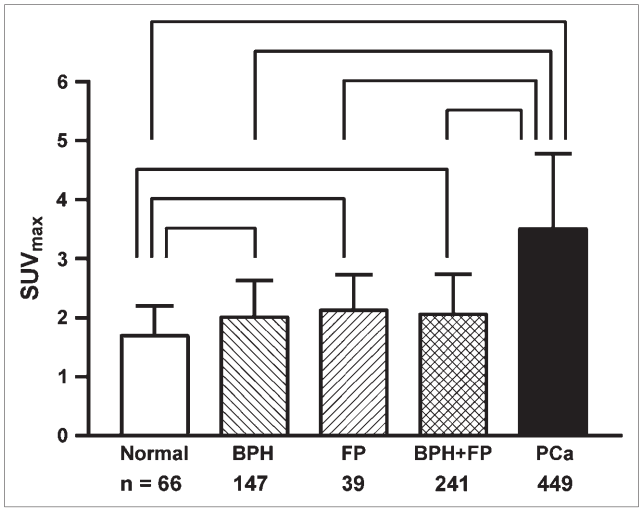

FIGURE 3. ^{11}C-Choline SUV_{max} in segments with normal prostate tissue, benign hyperplasia (BPH), focal prostatitis (FP), BPH mixed with focal prostatitis (BPH + FP), and segments with PCa. Data are expressed as mean ± SD, with significant differences (all with $P < 0.001$) indicated above histograms.

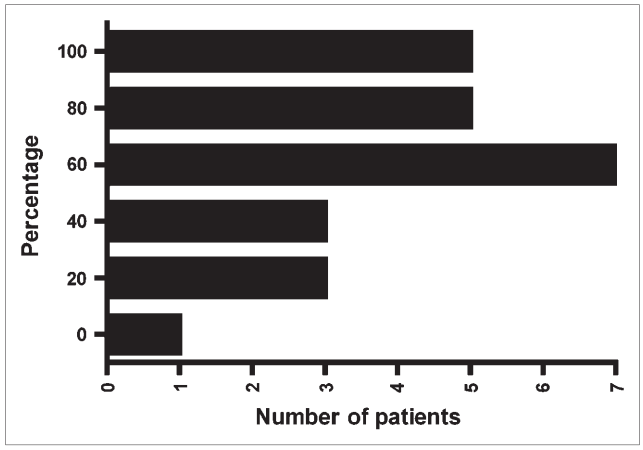

FIGURE 4. Percentage of segments in each patient with SUV_{max} PCa > SUV_{max} of benign histopathology (class width, 20%) vs. number of patients in respective class (2 patients are not listed because they had PCa in all segments).

The maximal segmental ^{11}C-choline SUV in all patients was not related to PSA or Gleason score. However, we did observe a weak, but significant, correlation of tumoral ^{11}C-choline SUV_{max} to pT stage (Fig. 5B; Spearman $r = 0.49$, $P = 0.01$).

DISCUSSION

Accurate imaging of cancer within the prostate may be important for patients with a clinical suspicion of PCa and negative core biopsies. Targeted repeated biopsy might improve the detection rate of PCa in these patients.

The results of this study indicate that ^{11}C-choline PET/CT identifies substantial tumor territories within the prostate gland in virtually all patients examined. Visual assessment and quantitative segmental analysis of ^{11}C-choline uptake detected PCa in 26 of 26 patients and 25 of 26 patients, respectively. In addition, a segmental SUV_{max} > 2.65 had an accuracy of 84% for correctly detecting segments with PCa. Accordingly, the area under the ROC curve of 0.89 indicated an accurate detection rate of cancer within the prostate gland. It might be prudent to consider that both sensitivity and specificity are influenced by the highly selected patient population with biopsy-proven PCa. However, we did not see any alternative to the selection process, as a close match of segmental mapping of histopathology and imaging was intended. Similar results were recently reported by Kwee et al. using a dual-phase ^{18}F-fluorocholine PET technique (*21*).

Nevertheless, there was some overlap of ^{11}C-choline uptake in segments with benign lesions and those with cancer, leading to an unreliable location by visual diagnosis of PCa in 1 of 26 patients. However, an imprecise assignment of PET/CT with histologic image plane cannot be excluded as a potential cause. Many small tumor areas with low ^{11}C-choline uptake—hidden within areas of normal tissue, hyperplasia, or focal prostatitis—will almost certainly

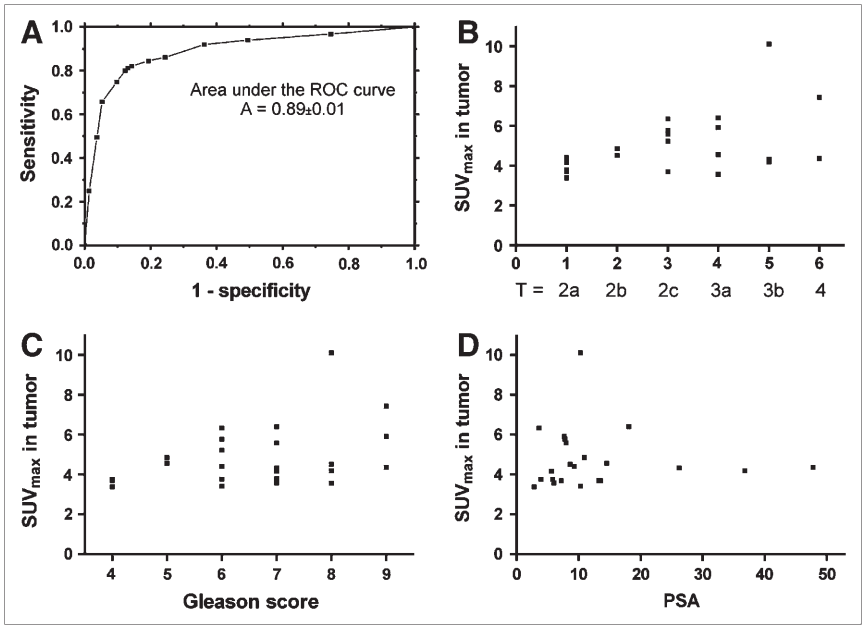

FIGURE 5. (A) ROC curve for correctly assigning PCa by segmental ^{11}C-choline uptake to segmental histopathologic examination. Maximal ^{11}C-choline uptake (SUV_{max}) is plotted against tumor stage (B), Gleason score (C), and serum PSA concentration (D). ^{11}C-Choline SUV_{max} showed weak, but significant, correlation with pT stage (Spearman $r = 0.49$; $P = 0.01$).

escape PET/CT detection. Some small tumor foci of <3–4 mm in cross-sectional diameter might have been missed on histology and are a potential source of inaccurate segmental PET/CT classifications. Because of the limited resolution and the 4.25-mm slice thickness of the imaging system, we do not see any possibility to correct for this inaccuracy. However, as long as combined with larger ^{11}C-choline PET/CT–positive tumor territories (observed in this study in 25 of 26 patients), small tumor areas not detected preoperatively are probably of minor concern as long as major tumor territories are accurately located and targeted biopsy is facilitated.

Increased ^{11}C-choline or ^{18}F-methylcholine uptake was observed in inflammatory lesions (*28*) and might contribute to the attenuated differentiation of benign from malignant tissue in some segments. Metabolically active, cytokine-stimulated tissue in segments with BPH (*29,30*) might also show upregulated choline metabolism and, thus, hamper differentiation of cancerous from benign tissue. However, we found that ^{11}C-choline uptake in benign hyperplasia and foci with chronic prostatitis were significantly lower than a substantial fraction of segments with PCa in nearly all patients.

We observed 86 false-negative segments of 449 segments with tumor involvement shown by histopathology (19.2%). From these 449 tumor-involved segments, 177 had tumor foci of >5 mm in diameter. In these 21 of 177 segments (11.8%), in which a clear ^{11}C-choline PET/CT signal would be expected, a false-negative imaging result may be due to a misalignment of imaging and prostate tissue cutting plane. The lower false-negative detection rate in the latter subgroup might be attributed to the increased tumor size.

We did not try to determine capsular infiltration with ^{11}C-choline PET/CT and believe that prediction of T staging with ^{11}C-choline PET/CT will be difficult or impossible because of the inherent physical limitations of the PET equipment used. Accordingly, microscopic infiltration of the bladder wall was not detected with ^{11}C-choline PET/CT in 1 patient, probably due to limited resolution of the imaging system. We observed substantial radioactivity content within the bladder in 9 of 26 patients, which might hamper imaging of the prostate when filtered backprojection and ^{68}Ge transmission data are used for image reconstruction. Use of an advanced iterative reconstruction algorithm in conjunction with low-noise CT data for transmission correction provided high-quality PET/CT images that could be exactly overlaid with the CT image set. Therefore, radioactivity uptake in the bladder or rectum could be easily differentiated from intraprostatic radioactivity distribution.

In agreement with Breeuwsma et al., we observed a weak correlation of maximal segmental SUV with tumor stage (*31*). Accordingly, we also observed a lower SUV_{max} in tumors of stage pT2a compared with those with stage > pT2a. This might suggest an association between the extent of PCa within the prostate and upregulation of choline metabolism in tumor tissue. In agreement with other authors, we did not observe a correlation of tumoral ^{11}C-choline SUV_{max} with serum PSA concentration, Gleason score, or Ki67 labeling index (*22,31,32*), indicating that biologic aggressiveness may not be a dominant influencing factor of choline metabolism in PCa (*31,32*). The weak correlation of ^{11}C-choline SUV_{max} with serum PSA reported by Yamaguchi et al. (*17*) might be influenced by a relatively large BPH-related component of the serum PSA concentration (*33*). Because of our recruitment strategy, there were no patients with T1a or T1b disease in the study population and all patients with T1c disease had a histopathologic diagnosis from the resected prostate. Therefore, results and conclusions of this study are limited to

stage ≥ T2a PCa. From a clinical perspective, ^{11}C-choline PET/CT might be used efficiently for stereotactic tissue sampling in patients with clinical suspicion of PCa and negative core biopsies. Farsad et al. (*22*) reported a similar approach, in which they successfully performed ^{11}C-choline PET/CT–guided rebiopsy in 3 of 36 patients, who had initially negative core biopsies.

CONCLUSION

The results of this study show that ^{11}C-choline is accumulated preferentially within PCa tissue, and major territories with PCa can be imaged precisely, located, and differentiated from benign tissue with ^{11}C-choline PET/CT. Provided that these findings are confirmed in a larger cohort, ^{11}C-choline PET/CT has the potential to improve the work-up and management of patients with primary cancer of the prostate.

REFERENCES

1. Jemal A, Murray T, Samuels A, Ghafoor A, Ward E, Thun MJ. Cancer statistics, 2005. *CA Cancer J Clin.* 2005;53:5–26.
2. Hara T, Kosaka N, Kishi H. PET imaging of prostate cancer using carbon-11-choline. *J Nucl Med.* 1998;39:990–995.
3. DeGrado TR, Coleman RE, Wang S, et al. Synthesis and evaluation of ^{18}F-labeled choline as an oncologic tracer for positron emission tomography: initial findings in prostate cancer. *Cancer Res.* 2001;61:110–117.
4. Hara T, Kosaka N, Kishi H. Development of ^{18}F-fluoroethylcholine for cancer imaging with PET: synthesis, biochemistry, and prostate cancer imaging. *J Nucl Med.* 2002;43:187–199.
5. Yu KK, Scheidler J, Hricak H, et al. Prostate cancer: prediction of extracapsular extension with endorectal MR imaging and three-dimensional proton MR spectroscopic imaging. *Radiology.* 1999;213:481–488.
6. Scheidler J, Hricak H, Vigneron DB, et al. Prostate cancer: localization with three-dimensional proton MR spectroscopic imaging—clinicopathologic study. *Radiology.* 1999;213:473–480.
7. Rodriguez-González A, Molina AR, Benitez-Rajal J, Lacal JC. Phospholipase D and choline kinase: their role in cancer development and their potential as drug targets. *Prog Cell Cycle Res.* 2003;5:191–201.
8. Rodriguez-González A, Molina AR, Fernández F, et al. Inhibition of choline kinase as a specific cytotoxic strategy in oncogene-transformed cells. *Oncogene.* 2003;22:8803–8812.
9. Ramirez de Molina A, Rodriguez-Gonzalez A, Gutierrez R, et al. Overexpression of choline kinase is a frequent feature in human tumor-derived cell lines and in lung, prostate, and colorectal human cancers. *Biochem Biophys Res Commun.* 2002;296:580–583.
10. Roivainen A, Forsback S, Gronroos T, et al. Blood metabolism of [methyl-^{11}C] choline: implications for in vivo imaging with positron emission tomography. *Eur J Nucl Med.* 2000;27:25–32.
11. Kotzerke J, Gschwend JE, Neumaier B. PET for prostate cancer imaging: still a quandary or the ultimate solution? *J Nucl Med.* 2002;43:200–202.
12. Kotzerke J, Volkmer BG, Neumaier B, Gschwend JE, Hautmann RE, Reske SN. Carbon-11 acetate positron emission tomography can detect local recurrence of prostate cancer. *Eur J Nucl Med Mol Imaging.* 2002;29:1380–1394.
13. Kotzerke J, Volkmer BG, Glatting G, et al. Intraindividual comparison of [^{11}C]acetate and [^{11}C]choline PET for detection of metastases of prostate cancer. *Nuklearmedizin.* 2003;42:25–30.
14. Kotzerke J, Prang J, Neumaier B, et al. Experience with carbon-11 choline positron emission tomography in prostate carcinoma. *Eur J Nucl Med.* 2000; 27:1415–1419.
15. de Jong IJ, Pruim J, Elsinga PH, Vaalburg W, Mensink HJ. Visualisation of prostate cancer with ^{11}C-choline positron emission tomography. *Eur Urol.* 2002; 42:18–23.
16. Picchio M, Messa C, Landoni C, et al. Value of [^{11}C]choline-positron emission tomography for re-staging prostate cancer: a comparison with [^{18}F] fluorodeoxyglucose-positron emission tomography. *J Urol.* 2003;169:1337–1340.
17. Yamaguchi T, Lee J, Uemura H, et al. Prostate cancer: a comparative study of ^{11}C-choline PET and MR imaging combined with proton MR spectroscopy. *Eur J Nucl Med Mol Imaging.* 2005;32:742–748.
18. de Jong IJ, Pruim J, Elsinga PH, Vaalburg W, Mensink HJ. Preoperative staging of pelvic lymph nodes in prostate cancer by ^{11}C-choline PET. *J Nucl Med.* 2003;44:331–335.
19. Kwee SA, Coel MN, Lim J, Ko JP. Prostate cancer localization with ^{18}fluorine fluorocholine positron emission tomography. *J Urol.* 2005;173:252–255.
20. Schmid DT, John H, Zweifel R, et al. Fluorocholine PET/CT in patients with prostate cancer: initial experience. *Radiology.* 2005;235:623–628.
21. Kwee SA, Wei H, Sesterhenn I, Yun D, Coel MN. Localization of primary prostate cancer with dual-phase ^{18}F-fluorocholine PET. *J Nucl Med.* 2006;47: 262–269.
22. Farsad M, Schiavina R, Castellucci P, et al. Detection and localization of prostate cancer: correlation of ^{11}C-choline PET/CT with histopathologic step-section analysis. *J Nucl Med.* 2005;46:1642–1649.
23. Wilson AA, Garcia G, Jin L, Houle S. Radiotracer synthesis from [^{11}C]iodomethane: a remarkably simple captive solvent method. *Nucl Med Biol.* 2000;27: 529–532.
24. Holmberg L, Bill-Axelson A, Helgesen F, et al. A randomized trial comparing radical prostatectomy with watchful waiting in early prostate cancer. *N Engl J Med.* 2002;347:781–789.
25. Wittekind C, Meyer H, Bootz F. *TNM: Klassifikation maligner Tumoren*. 6th ed. Berlin, Germany: Springer Verlag; 2003.
26. Beard CJ, Kijewski P, Bussiere M, et al. Analysis of prostate and seminal vesicle motion: implications for treatment planning. *Int J Radiat Oncol Biol Phys.* 1996; 34:451–458.
27. Metz CE. ROC methodology in radiologic imaging. *Invest Radiol.* 1986;21: 720–733.
28. Wyss MT, Weber B, Honer M, et al. ^{18}F-Choline in experimental soft tissue infection assessed with autoradiography and high-resolution PET. *Eur J Nucl Med Mol Imaging.* 2004;31:312–316.
29. Untergasser G, Madersbacher S, Berger P. Benign prostatic hyperplasia: age-related tissue-remodeling. *Exp Gerontol.* 2005;40:121–128.
30. Huang X, Lee C. Regulation of stromal proliferation, growth arrest, differentiation and apoptosis in benign prostatic hyperplasia by TGF-beta. *Front Biosci.* 2003;8:S740–S749.
31. Breeuwsma AJ, Pruim J, Jongen MM, et al. In vivo uptake of [^{11}C]choline does not correlate with cell proliferation in human prostate cancer. *Eur J Nucl Med Mol Imaging.* 2005;32:668–673.
32. Sutinen E, Nurmi M, Roivainen A, et al. Kinetics of [^{11}C]choline uptake in prostate cancer: a PET study. *Eur J Nucl Med Mol Imaging.* 2003;31:317–324.
33. Grall J, Corbel L. PSA and benign prostatic hyperplasia. *Ann Urol (Paris).* 2004;38:S43–S45.

JNM The Journal of NUCLEAR MEDICINE

Imaging Prostate Cancer with ^{11}C-Choline PET/CT

Sven N. Reske, Norbert M. Blumstein, Bernd Neumaier, Hans-Werner Gottfried, Frank Finsterbusch, Darius Kocot, Peter Möller, Gerhard Glatting and Sven Perner

J Nucl Med. 2006;47:1249-1254.

The Journal of Nuclear Medicine is published monthly.
SNMMI | Society of Nuclear Medicine and Molecular Imaging
1850 Samuel Morse Drive, Reston, VA 20190.
(Print ISSN: 0161-5505, Online ISSN: 2159-662X)

SNMMI SOCIETY OF NUCLEAR MEDICINE AND MOLECULAR IMAGING